BIOCHEMISTRY
including biophysical chemistry & molecular biology

ARTICLE

pubs.acs.org/biochemistry

Zinc Inhibition of Bacterial Cytochrome bc_1 Reveals the Role of Cytochrome *b* E295 in Proton Release at the Q_o Site

Dong-Woo Lee,[†,⊥] Youssef El Khoury,[‡] Francesco Francia,[§] Barbara Zambelli,[∥] Stefano Ciurli,[∥] Giovanni Venturoli,[§] Petra Hellwig,[‡] and Fevzi Daldal*[,†]

[†]Department of Biology, University of Pennsylvania, Philadelphia, Pennsylvania 19104, United States

[‡]Institut de Chimie, UMR 7177, Laboratoire de Spectroscopie Vibrationnelle et Electrochimie des Biomolécules, Université de Strasbourg, 67070 Strasbourg, France

[§]Laboratorio di Biochimica e Biofisica, Dipartimento di Biologia, Università di Bologna, 40126 Bologna, Italy

[∥]Laboratory of Bioinorganic Chemistry, University of Bologna, 40127 Bologna, Italy, and Center for Magnetic Resonance, University of Florence, Florence, Italy

ABSTRACT: The cytochrome (cyt) bc_1 complex (cyt bc_1) plays a major role in the electrogenic extrusion of protons across the membrane responsible for the proton motive force to produce ATP. Proton-coupled electron transfer underlying the catalysis of cyt bc_1 is generally accepted, but the molecular basis of coupling and associated proton efflux pathway(s) remains unclear. Herein we studied Zn^{2+}-induced inhibition of *Rhodobacter capsulatus* cyt bc_1 using enzyme kinetics, isothermal titration calorimetry (ITC), and electrochemically induced Fourier transform infrared (FTIR) difference spectroscopy with the purpose of understanding the Zn^{2+} binding mechanism and its inhibitory effect on cyt bc_1 function. Analogous studies were conducted with a mutant of cyt *b*, E295, a residue previously proposed to bind Zn^{2+} on the basis of extended X-ray absorption fine-structure spectroscopy. ITC analysis indicated that mutation of E295 to valine, a noncoordinating residue, results in a decrease in Zn^{2+} binding affinity. The kinetic study showed that wild-type cyt bc_1 and its E295V mutant have similar levels of apparent K_m values for decylbenzohydroquinone as a substrate (4.9 ± 0.2 and 3.1 ± 0.4 μM, respectively), whereas their K_I values for Zn^{2+} are 8.3 and 38.5 μM, respectively. The calorimetry-based K_D values for the high-affinity site of cyt bc_1 are on the same order of magnitude as the K_I values derived from the kinetic analysis. Furthermore, the FTIR signal of protonated acidic residues was perturbed in the presence of Zn^{2+}, whereas the E295V mutant exhibited no significant change in electrochemically induced FTIR difference spectra measured in the presence and absence of Zn^{2+}. Our overall results indicate that the proton-active E295 residue near the Q_o site of cyt bc_1 can bind directly to Zn^{2+}, resulting in a decrease in the electron transferring activity without changing drastically the redox potentials of the cofactors of the enzyme. We conclude that E295 is involved in proton efflux coupled to electron transfer at the Q_o site of cyt bc_1.

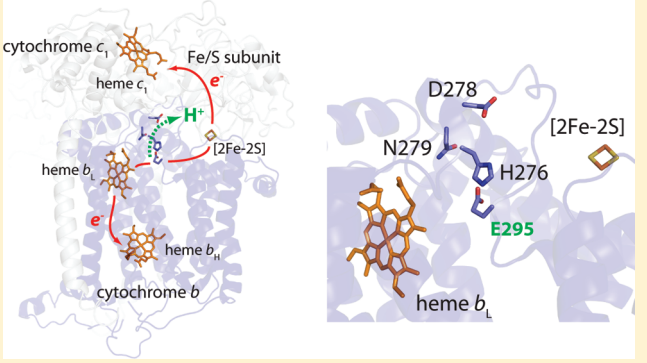

In the respiratory and photosynthetic chains of organisms, electrons are transferred sequentially from low-redox potential donors to high-redox potential acceptors, in events coupled to the translocation of a proton across the membrane. The process maintains a transmembrane electrochemical proton gradient (ΔpH), which is used to drive the synthesis of ATP.[1,2] The concerted movement of protons and electrons is a common feature of many energy-transducing complexes, including the photosynthetic reaction center (RC), cytochrome (cyt) bc_1 complex (cyt bc_1), and cyt *c* oxidase (Cox). Among them, cyt bc_1 is one of the components that generates a proton gradient across the membrane by the uptake and release of protons on both sides of the lipid bilayer in a manner coupled to electron transfer.[3,4] According to the Q cycle mechanism, a hydroquinone (QH_2) molecule is oxidized at a QH_2-oxidizing (Q_o) site of cyt bc_1 to produce two electrons. The first electron goes to the high-potential chain comprised of the Rieske Fe−S protein and cyt c_1, while the other electron enters into a low-potential chain fully confined to cyt *b* hemes b_L and b_H.[5−8] Eventually, the high-potential chain in phototrophic bacteria conveys the first electron from QH_2 to a terminal acceptor (i.e., either Cox in respiration or a photo-oxidized RC in photosynthesis) via cyt c_2 (and cyt c_y in *Rhodobacter capsulatus*).[9−11] The second electron from QH_2 is transferred to the Q_i site via the two hemes, b_L and b_H, to reduce a Q to an intermediate SQ.[3,12] Upon oxidation of a second QH_2 at a Q_o site, another electron is used to reduce the SQ at the Q_i site

Received: February 14, 2011
Revised: April 16, 2011
Published: April 18, 2011

to QH_2. Consequently, a complete turnover of cyt bc_1 consumes one Q and two protons at the n side of the membrane to generate a QH_2, an event concomitant with oxidation of two QH_2 molecules at the Q_o site(s) to release four protons to the p side of the membrane, resulting in the formation of a proton gradient (ΔpH) and a membrane potential ($\Delta\psi$) across the membrane. The bifurcated electron transfer reaction at the Q_o site between the high- and low-potential chains of the enzyme is a unique functional characteristic of cyt bc_1 through which the free energy difference between Q_{pool} and the electron acceptor is used to generate ΔpH and $\Delta\psi$. In membrane proteins, protons are known to move through ordered chains of water, but how the rate and direction of proton movement is controlled and coordinated with coupled electron transfer is not understood. In particular, little is known about the proton uptake and release events of cyt bc_1.

Several approaches have been used to identify the proton transfer pathway(s), starting with cyt *b*, which plays a key role in both electron transfer and proton release and uptake activities.[13−15] Initially, the use of dicyclohexylcarbodiimide (DCCD), a well-known carboxyl-modifying reagent, suggested that the cyt *b* D187 residue of *Rhodobacter sphaeroides* cyt bc_1 might be involved in proton translocation.[13] Subsequent studies[15] demonstrated that this residue was unlikely to be involved in the protonogenic reactions of cyt bc_1. Rather, DCCD caused inhibition of the Fe−S protein-mediated electron transfer reactions between the Q_o site and cyt c_1 as well as the QH_2 oxidation at the Q_o site.[14] Molecular modeling studies of DCCD-treated cyt bc_1 proposed that conformational changes caused by DCCD binding to E163 (mitochondrial numbering) in the cd_2 loop of cyt *b* of chicken cyt bc_1 could generate new hydrogen bonds between E272 and D253 and Y274 residues to affect the rotation and protonation of E272 (corresponding to *R. capsulatus* E295),[16] which was thought to be important for capturing a proton derived from QH_2 oxidation at the Q_o site.[17] Nevertheless, the proton transfer pathway in the bacterial cyt bc_1 still remains unclear.

Earlier observations have indicated that transition metal ions such as Zn^{2+} and Cd^{2+} can inhibit the proton transfer activity of the bacterial RC.[18−20] When Zn^{2+} binds to the RC, the rate of transfer of a proton to E212 of RC subunit L was decreased, becoming a rate-limiting step.[20] In addition, the X-ray crystal structure of the RC bound to Zn^{2+} revealed that the Zn^{2+} binding cluster of D124, H126, and H128 of RC subunit H was involved in the pathway of the delivery of the first proton to Q_B^- at the entry point.[21] Furthermore, the second proton supplied to $(Q_BH)^-$ by E212 also shares the same entry point of the first proton, close to the metal binding cluster.[20] Similarly, the proton uptake pathways (i.e., the D and K channels) in Cox were studied using Zn^{2+} and Cd^{2+} binding experiments.[22,23] These and other related works indicated that identification of transition metal binding sites in energy-transducing components provides an incisive approach to identifying the residues involved in proton transfer pathways. Previously, we probed the local structure of Zn^{2+} bound stoichiometrically to noncrystallized cyt bc_1 species purified from bacteria and mitochondria using Zn K-edge extended X-ray absorption fine-structure spectroscopy (EXAFS),[24] which provided results consistent with the crystal structures of the same cyt bc_1 forms bound to Zn^{2+}.[25] EXAFS data demonstrated that the *R. capsulatus* cyt bc_1 Zn^{2+} binding site exhibited a distinct hexacoordination and pseudo-octahedral geometry, which included residues H276, D278, N279, and E295. This binding mode is different from the four-coordinate tetrahedral Zn^{2+} binding site observed in the mitochondrial cyt bc_1 species, but remarkably, the locus of metal ion binding was identical (Figure 1). The metal binding residues are close to the p side of the membrane surface, suggesting that this locus could represent the proton exit domain(s) of the Q_o site. In light of the earlier works suggesting that mitochondrial E272 (E295 in *R. capsulatus* cyt bc_1) is tightly involved in QH_2 oxidation,[17,26] we examined the effect of Zn^{2+} binding to cyt bc_1. We conducted inhibitory kinetics, isothermal titration calorimetry analyses, and electrochemically induced Fourier transform infrared (FTIR) difference spectroscopy with the wild-type (WT) enzyme and its E295V mutant variant in the presence and absence of Zn^{2+}. Our overall findings indicate that the Zn^{2+} binding ligand E295 of cyt *b* affects the catalytic activity (i.e., k_{cat}) of cyt bc_1, suggesting that it modulates rapid electron transfer in a manner coupled to the release of a proton from the Q_o site of the enzyme.

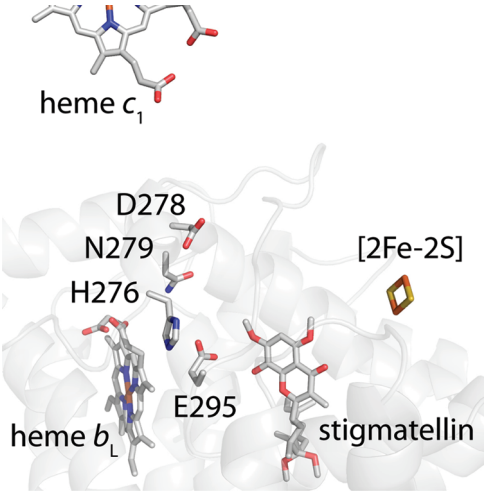

Figure 1. Close-up of the three-dimensional structure of the cyt *b* subunit of *R. capsulatus* cyt bc_1 bound with stigmatellin (Protein Data Bank entry 1ZRT).[49] For visual convenience, the Fe−S protein and cyt c_1 catalytic subunits have been omitted. The cyt *b* subunit (gray) is rendered transparent, and its H276, D278, N279, and E295 residues proposed to act as Zn^{2+} ligands[24] are shown as sticks. The [2Fe-2S] cluster, hemes b_L and c_1, and the Q_o site inhibitor stigmatellin are shown as sticks.

MATERIALS AND METHODS

Growth Conditions and Purification of cyt bc_1. *R. capsulatus* strains were grown at 35 °C in mineral-peptone-yeast extract (MPYE) enriched medium supplemented with 10 μg/mL kanamycin under semiaerobic and dark respiratory conditions.[27] The wild-type and mutant cyt bc_1, as well as the two-subunit cyt bc_1 subcomplex lacking the Fe−S protein, were purified from chromatophore membranes derived from cells grown under the respiratory conditions as described previously.[28,29] Briefly, chromatophore membranes prepared in 50 mM Tris-HCl buffer (pH 8.0) and 100 mM NaCl were solubilized with dodecyl maltoside (DDM) to a final concentration of 1 mg of DDM/mg of total proteins. The mixture was stirred gently for 1 h at 4 °C and then ultracentrifuged (120000*g* for 2 h) to eliminate non-dispersed membranes. The supernatant was loaded onto a DEAE-Biogel A column (2.6 cm × 32 cm) pre-equilibrated with 50 mM Tris-HCl buffer (pH 8.0) containing 20% glycerol, 0.01% (w/v) DDM, and 100 mM NaCl (buffer A). The column was washed with 5−6 column volumes (CVs) of buffer A containing

150 mM NaCl, and then the remaining photosynthetic pigments were washed with 3−4 CVs of the same buffer until a red band on top of the column became visible. The adsorbed cyt bc_1 proteins were eluted with 4 CVs of a linear 150 to 400 mM NaCl gradient in the presence of 0.01% (w/v) DDM. Fractions were monitored for their absorption at 280 and 420 nm, and at 500−600 nm for their dithionite-reduced minus ferricyanide-oxidized optical difference spectra, and those containing the highest concentrations of *c*- and *b*-type cyts were pooled and concentrated using an Amicon Diaflo apparatus equipped with a PM30 membrane. The concentrated sample (∼2 mL) was passed through a Sephacryl S400 size-exclusion column (405 mL), pre-equilibrated with 10 CVs of 50 mM Tris-HCl buffer (pH 8.0) containing 150 mM NaCl, 20% glycerol, and 0.01% (w/v) DDM. Fractions containing cyt bc_1 were pooled, concentrated using Amicon Ultra (50K molecular weight cutoff) centrifugal filter devices (Millipore Co.), and stored at −80 °C in the presence of 20% glycerol until further use. The concentration of cyt bc_1 was estimated from reduced minus oxidized difference spectra with an extinction coefficient of 28.5 mM^{-1} cm^{-1} for the dithionite-reduced cyt *b* (at 560 nm vs 570 nm).[29] Protein concentrations were determined using the bicinchoninic acid method[30] with bovine serum albumin as a standard. Sodium dodecyl sulfate−polyacrylamide gel electrophoresis (15%) was conducted as described in ref 31, and prior to being loaded, samples were solubilized in 62.5 mM Tris (pH 6.8), 2% SDS, 0.1 M dithiothreitol, 25% glycerol, and 0.01% bromophenol blue with subsequent incubation at 60 °C for 10 min.

Enzyme Kinetics. Decylbenzohydroquinone (DBH_2):cyt reductase assays were performed as described in ref 29. Reaction mixtures (2 mL) contained 50 mM sodium phosphate buffer (pH 7.4), 40 μM horse heart cyt *c*, 2 mM KCN, 0.1 g/L DDM, and 2.3 nM purified cyt bc_1. The reductase reaction was started by addition of DBH_2 in dimethyl sulfoxide (final concentration of 40 μM). Michaelis−Menten kinetics was performed as described above in a stirred cuvette thermostated at 20 °C using various concentrations of DBH_2 as a substrate ranging from 0.5 to 40 μM. The decylbenzoquinone (DB) concentration was determined spectroscopically using an extinction coefficient of 16 mM^{-1} cm^{-1}, and the solution is fully reduced with sodium borohydride.[32] For Zn^{2+} inhibition kinetics, up to 0.2 mM $ZnSO_4$ from stock solutions of 0.1, 1, 10, or 100 mM (2−10 μL) was added to the reaction mixtures containing 2.3 nM purified cyt bc_1 in a stirred cuvette to give the desired final concentration and preincubated for 1 min before the reaction was started by the addition of 40 μM DBH_2. Thereafter, the reduction of cyt *c* was monitored at 550 nm for 1 min to yield an initial rate of the enzyme reaction. One unit of cyt bc_1 activity was defined as the amount of enzyme that produced 1 μmol of reduced cyt *c*/min under the assay conditions.

Isothermal Titration Calorimetry Analysis. Zn^{2+} titration experiments were performed at 25 °C using a high-sensitivity VP-ITC microcalorimeter (MicroCal LLC, Northampton, MA). The $ZnSO_4$ solutions were prepared in 50 mM Tris-HCl buffer (pH 8.0) containing 150 mM NaCl, 20% glycerol, and 0.01% (w/v) DDM, yielding final concentrations ranging from 350 to 700 μM. The reference cell was filled with deionized water. Each experiment was started with a small injection of 1−2 μL, which was discarded from the analysis of the integrated data, to prevent artifacts due to the diffusion through the injection port occurring during the long equilibration period, locally affecting the protein concentration near the syringe needle tip. Care was taken to start the first addition after baseline stability had been achieved. In each individual titration, 5 μL of the $ZnSO_4$ solution was injected into a solution of the wild-type and E295V mutant cyt bc_1 (10−12 μM) diluted in the same buffer using a computer-controlled 310 μL microsyringe. Allowing a time interval of 300 s between each Zn^{2+} injection ensured chemical equilibrium of the system. For a control experiment, the metal solution without enzyme was titrated under the same conditions. Integrated heat data were fitted by a nonlinear least-squares minimization algorithm using MicroCal Origin.

FTIR Spectroscopic Analysis. FTIR difference spectra were recorded as a function of the applied potential using a Vertex 70 spectrometer (Bruker Optics) equipped with an MCT detector and a globar light source. The difference spectra were recorded in the 1800−800 cm^{-1} range using a previously described electrochemical cell.[33] Although using ZnSe windows instead of CaF_2 allow the difference spectra to be recorded from 1800 to 650 cm^{-1}, here the spectra were recorded between 1800 and 800 cm^{-1}.[34] To accelerate the redox reaction, we used a mixture of mediators as described previously.[35] The protein was equilibrated at an initial electrode potential, and a single-beam spectrum was recorded. Then the final potential was applied, and a single-beam spectrum was again recorded after equilibration. Equilibration generally took less than 10 min for the full potential step from −0.292 to 0.708 V versus the standard hydrogen electrode (SHE). The difference spectra presented here were calculated from two single-beam spectra, with the initial spectrum taken as a reference. Typically, 2 × 256 interferograms at 4 cm^{-1} resolution were co-added for each single-beam spectrum and Fourier-transformed using triangular apodization and a zero-filling factor of 2. At least 35 difference spectra were averaged.

UV−Vis Spectroscopic Analysis. The UV−vis difference spectra of all the samples were recorded on a Cary 300 spectrometer using the same electrochemical cell as for the FTIR difference spectroscopy equipped with CaF_2 windows. The UV−vis potentiometic oxidative titrations of the cyt bc_1 samples were performed by following the evolution of the Soret band of the heme absorbance. The absorbance values were then plotted versus the applied potential.

RESULTS

Kinetics of Wild-Type and cyt *b* E295V Mutant cyt bc_1. The kinetic parameters of wild-type cyt bc_1 were studied and compared with those of its E295V mutant derivative. First, to establish the ratio of enzyme to substrate (i.e., cyt bc_1 vs DBH_2) necessary to have a reliable initial velocity, we monitored the reduction of horse heart cyt *c* (the electron acceptor) at different DBH_2 concentrations (the electron donor) at 550 nm under standard assay conditions. The study demonstrated that both the wild-type enzyme and its E295V mutant exhibited good linearity of the reaction rate over a 1 min interval using an [S]/[E] ratio of $>10^4$. We analyzed the kinetic data to determine the K_m values for DBH_2 and V_{max} using double-reciprocal plots and fit the data with a simple Michaelis−Menten equation (Table 1). The wild-type cyt bc_1 featured a K_m of 4.9 μM for DBH_2 as a substrate and a V_{max} value of 42.4 μmol min^{-1} mg^{-1}. The E295V mutant had a slightly lower K_m value (3.1 μM) than the wild-type. This value is similar to that of the E272Q mutant of yeast cyt bc_1 (3.2 μM)[36] and is slightly lower than that of the yeast cyt bc_1 E272V mutant (4.2 μM),[37] indicating that the E295V mutation does not cause

Table 1. Kinetic Parameters of cyt bc_1 from *R. capsulatus* and Various Organisms

enzyme source		K_m (μM)	V_{max} (μmol min^{-1} mg^{-1})	k_{cat} (s^{-1})	V_{max}/K_m (μmol min^{-1} mg^{-1} μM^{-1})	ref
R. capsulatus[a]	WT	4.9 ± 0.2[b]	42.4 ± 0.8	85.2 ± 13.1	8.6	this study
	E295V	3.1 ± 0.4	10.6 ± 0.4	34.3 ± 4.5	3.4	
Saccharomyces cerevisiae[a]	WT	6.3	ND[c]	52.1 ± 5.0	ND[c]	36
	E272Q	3.2	ND[c]	6.9 ± 1.0	ND[c]	
S. cerevisiae	WT	4	ND[c]	61	(15.3)[d]	37
	E272V	4.2	ND[c]	26	(6.2)[d]	

[a] Determined with the purified enzyme. [b] Data are means ± standard deviations. [c] Not determined. [d] Note that these numbers correspond to K_{min} (k_{cat}/K_m) as defined in ref 37 and not to V_{max}/K_m.

any significant difference in the QH_2 binding affinity, a finding that is consistent with previous EPR data for different E295 mutants.[26] It has been shown, using light-activated kinetics with chromatophore membranes derived from *R. capsulatus*, that the E295V mutant exhibits an ~4-fold decrease in the rate of heme b_H reduction.[26] Similar decreases in V_{max} for E295V compared to that of the wild-type were observed in this work (Table 1). The kinetic data thus confirmed that the E295V substitution did not alter significantly the binding affinity of QH_2 molecules at the Q_o site of cyt bc_1, but it rather decreased conspicuously the catalytic efficiency (V_{max}/K_m) of the enzyme during Q_o catalysis. This result implies that substitution of E295 to *V* perturbs the Q_o site, generating a rate-limiting step in either electron or proton transfer. The observation that the yeast E272V or bacterial E295V mutant did not show any significant effect on the Q_i site-mediated reverse electron transfer rate[37] or the Q_o site-mediated cyt b_H reduction rates,[26] respectively, suggests that no alteration of the electron transfer pathway is caused by the E295V mutation. In addition, the physicochemical properties of cyt bc_1 (i.e., $E_{m,7}$ of hemes b_L and b_H or redox sensitive spectra) were not altered by mutation of E295 in bacterial cyt bc_1.[26,38] On the other hand, the rate of reduction of b_H of E295Q at different pH values in bacterial mutants[26] and the turnover rate of cyt *c* reduction in E272D and Q at pH <6 in yeast[36] mutants were significantly decreased as compared to those of the corresponding wild-type enzymes. These findings pointed out that the observed catalytic defect might be linked to the proton-active carboxylate group of E295, although this effect was not seen with the yeast E272P and E272V mutants.[37]

Zn^{2+} Inhibition Kinetics of cyt bc_1. Previous EXAFS spectroscopy of Zn^{2+} stoichiometrically bound to cyt bc_1,[24] together with several other studies,[17,26,36−39] suggested that steps of protonation and deprotonation of E295 are closely linked to the rate-limiting Q_o site proton exchange. The Zn^{2+} binding assay using eukaryotic cyt bc_1 suggested that this enzyme has multiple independent Zn^{2+} binding sites with different affinities.[39] From the binding assay with radiolabeled Zn^{2+}, bovine cyt bc_1 was found to have two types of binding sites with different stoichiometries and affinities at pH 7.2: a high-affinity site (n = 1.1 ± 0.1 Zn^{2+}/c_1; K_I = 0.13 μM) and several low-affinity sites (n = 3−4 Zn^{2+}/c_1; K_I = 2.3 μM).[39] Chicken cyt bc_1 has a higher K_I (3 μM) than the bovine enzyme, and crystallographic studies initially indicated two different Zn^{2+} binding sites.[25] However, subsequent analyses revealed that it has only one site (see Protein Data Bank entry 3h1k, remark 280). Accordingly, Zn^{2+}-inhibitory kinetics studies were performed with purified bacterial wild-type and E295V mutant enzymes at various Zn^{2+} concentrations. Simple inhibition curves were obtained when purified *R. capsulatus* cyt bc_1 was titrated with Zn^{2+} in 40 mM Tris-HCl buffer (Figure 2). The inhibition curves were fitted by a

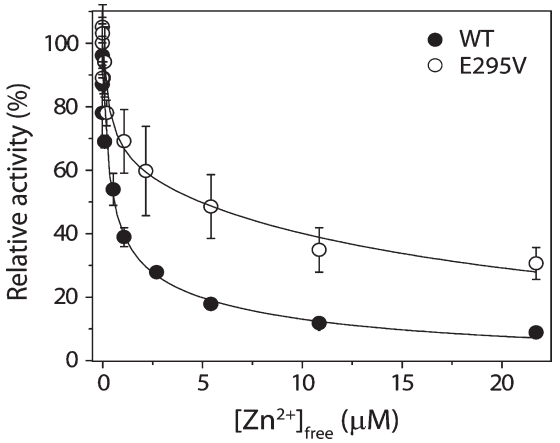

Figure 2. Inhibition of purified *R. capsulatus* cyt bc_1 by Zn^{2+}. DBH_2:cyt *c* oxidoreductase activities of the wild-type and E295V mutant enzymes with a DBH_2:cyt bc_1 concentration ratio of $>10^4$ were assayed at various Zn^{2+} concentrations in 40 mM Tris-HCl buffer (pH 7.5). Relative wild-type and E295V mutant enzyme activities observed in the presence of increasing concentrations of Zn^{2+} are shown with uninhibited 100% activities being approximately 31 and 10 μmol of cyt *c* reduced min^{-1} mg^{-1}, respectively (Table 1). The concentration of free Zn^{2+} in the Tris-HCl buffer was obtained from the equation $[Zn]_{free} = [Zn]_o/(1 + [Tris]_o/K_{Tris})$, where $[Zn]_o$ and $[Tris]_o$ are the initial concentrations of zinc and Tris, respectively, and K_{Tris} = 2.3 ± 0.2 mM.[50]

standard inhibition equation assuming either one or two independent type(s) of inhibition site(s). The K_I could be obtained by fitting the Zn^{2+} dependence with a single homogeneous inhibition site: $v = V_{max}/(1 + [Zn^{2+}]/K_I)$ (eq 1). At >0.2 mM Zn^{2+}, only 10% of the original activity remained (Figure 2), but there was no additional decrease in activity up to 0.6 mM Zn^{2+}. In 40 mM Tris-HCl buffer at pH 7.5, wild-type cyt bc_1 exhibited a K_I value of 0.9×10^{-6} M for Zn^{2+}, which is lower than that of chicken cyt bc_1.[25] On the other hand, E295V exhibited a K_I value of 2.6×10^{-6} M, which is approximately 3-fold higher than that of the wild-type (Figure 2 and Table 2). In addition, some residual activity (30%) of E295V was observed even at >0.2 mM Zn^{2+}. The Zn^{2+} binding affinities of the wild-type and the mutant cyt bc_1 derivative were determined more directly using microcalorimetry.

Zn^{2+} Binding Properties of cyt bc_1 Studied by Isothermal Titration Calorimetry. ITC measurements were taken with a goal of (i) detecting, using an independent approach, the presence of a high-affinity Zn^{2+} binding site in wild-type cyt bc_1, (ii) determining the dissociation constant (K_D) of the Zn^{2+} complex, and (iii) comparing the binding properties of wild-type cyt bc_1 with those of the E295V mutant derivative. The ITC

Table 2. Inhibition of Purified cyt bc_1 by Zn^{2+}

enzyme source	K_I (M)	K_D (M)	complete inhibition (μM)	ref
bovine	10^{-7} (pH 7.0)	10^{-7} (pH 7.0), $>2 \times 10^{-6}$	$[Zn^{2+}] > 5$	39
avian	3×10^{-6}	not determined	200 ($\leq$20%)	25
bacteria	0.9×10^{-6} (pH 7.5)	0.5×10^{-6}	200 ($\leq$10%)	this study

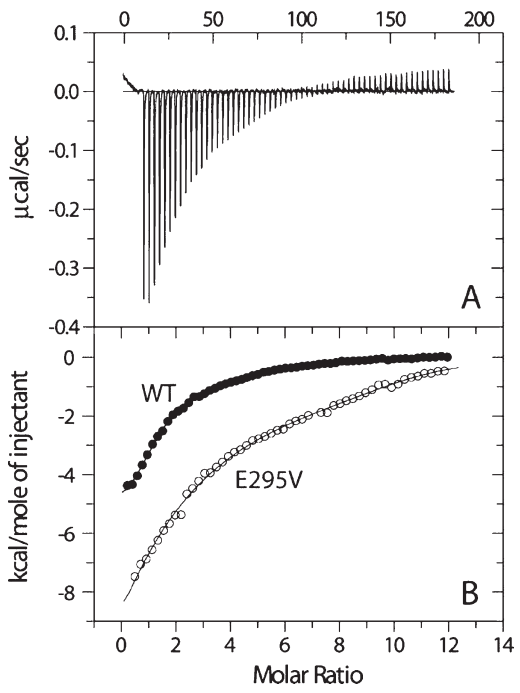

Figure 3. Binding of Zn^{2+} to wild-type and E295V cyt bc_1 as determined by ITC titrations. (A) Raw titration data represent the thermal effect of 5 μL injections of 500 μM Zn^{2+} into a solution of 9.7 μM wild-type enzyme. (B) Normalized heats of reaction, derived from the integration of raw data (like those shown in panel A for the wild-type), as a function of the Zn^{2+}:cyt bc_1 molar ratio, for the wild-type (●) and E295V mutant (○) cyt bc_1 enzymes. The total protein concentrations were 9.7 and 11.1 μM for the titrations performed with the wild-type and E295V mutant enzyme, respectively. The solid lines represent the best fits of the integrated data to a model that includes two noninteracting sets of binding sites. The corresponding values of the number of sites per protein complex and of the dissociation constants are as follows: $n_1 = 1.13 \pm 0.03$, $K_{D1} = 0.50 \pm 0.07$ μM, $n_2 = 3.7 \pm 0.2$, and $K_{D2} = 6.8 \pm 0.9$ μM for the wild-type, and $n_1 = 1$ (fixed), $K_{D1} = 1.00 \pm 0.36$ μM, $n_2 = 9.1 \pm 0.5$, and $K_{D2} = 3.5 \pm 1.6$ μM for the E295V mutant. See the text for further details.

measurements were performed by adding Zn^{2+} to the cyt bc_1 suspensions in the Tris-HCl buffer (pH 7.5). The occurrence of binding events was revealed by the presence of exothermic peaks that followed each Zn^{2+} addition as shown in Figure 3A. The titrations obtained from the integrated heat data for the wild-type and E295V mutant cyt bc_1 enzymes are compared in Figure 3B. Titrations were fitted to two different models characterized either by a single set or by two sets of independent, noninteracting binding sites. Each set had a number (n) of binding sites per protein complex, possessing the same intrinsic dissociation constant (K_D). Both in the wild-type and in the E295V mutant enzyme, the inclusion of a second binding event improved significantly the quality of the fit. When the data were fitted by using the two-site model equation, wild-type cyt bc_1 [Figure 3B (●)] had two K_D values of 0.5×10^{-6} M ($K_{D1} = 0.50 \pm 0.07$ μM) and 6.8×10^{-6} M ($K_{D2} = 6.8 \pm 0.9$ μM) with a stoichiometry n_1 of 1.13 ± 0.03 for the high-affinity site and a stoichiometry n_2 of 3.7 ± 0.2 for a few lower-affinity binding sites (Figure 3B and Table 2). The two binding events are driven by favorable enthalpic factors ($\Delta H_1 = -5.6 \pm 0.2$ kcal/mol, and $\Delta H_2 = -1.4 \pm 0.2$ kcal/mol, respectively). A second independent set of data (not shown) acquired for the wild-type enzyme at a comparable concentration of total protein yielded a titration essentially coincident with that shown in Figure 3B, indicating that the results were highly reproducible. It has been noted that the K_D of the high-affinity Zn^{2+} binding site of bovine cyt bc_1 was essentially identical to the inhibition constant (K_I) under all conditions tested.[39] A similar situation is found here for bacterial cyt bc_1. Zn^{2+} binds stoichiometrically to a high-affinity cyt bc_1 site, characterized by a dissociation constant, K_D (0.5×10^{-6} M), that is on the same order of magnitude as the K_I (0.9×10^{-6} M) determined by measuring the inhibition kinetics of Zn^{2+} under similar conditions (Figure 2). Therefore, we infer that binding of Zn^{2+} to the high-affinity site of cyt bc_1 caused its inhibition, whereas the additional low-affinity binding sites did not seem to induce additional inhibition of the catalytic activity. The presence of a few low-affinity binding sites was also detected in eukaryotic cyt bc_1.[39]

A quite distinct binding ITC pattern was observed in the E295V mutant, for which the titration [Figure 3B (○)] suggested that saturation of Zn^{2+} binding is attained at higher metal:protein ratios. Again, as observed in the wild-type complex, the one-site model was unable to describe adequately the titration, revealing the presence of additional binding sites. A blind fit to the data according to the two-site model, in which the free parameters of the fit were the number of binding sites (n_i), the enthalpy change (ΔH_i), and the dissociation constant (K_{Di}) (for each set i of binding sites), yielded an n_1 of 1.97 ± 0.08 and a K_D of 0.55 ± 0.09 μM for the higher-affinity set, with a ΔH_1 of -9.9 ± 0.7 kcal/mol, and 7.1 ± 0.3 (n_2) of low-affinity binding sites per cyt bc_1, characterized by a K_{D2} of 5.81 ± 1.22 μM and a ΔH_2 of -2.6 ± 0.3 kcal/mol. However, an equivalently good fit to the data, as judged from the essentially unaffected χ^2 value, could be obtained by reducing the number of free parameters, i.e., by fixing the stoichiometry of a set of binding sites to a unitary value, as found in the case of wild-type cyt bc_1 for the high-affinity site. This choice resulted in a stoichiometric high-affinity binding site characterized by a K_{D1} of 1.0×10^{-6} M (1.00 ± 0.36 μM) and an enthalpy change ΔH_1 of -28 ± 4 kcal/mol, in addition to 9.1 ± 0.5 (n_2) low-affinity sites characterized by a K_{D2} of 3.5×10^{-6} M (3.5 ± 1.6 μM) and a ΔH_2 of -0.9 ± 0.5 kcal/mol. Although the two fits are essentially equivalent on a purely statistical basis, the physical interpretation of the latter fit is simpler, because it appears rather unlikely that the substitution of E295 leads to the high-affinity binding of two Zn^{2+} ions in the same binding pocket or in its vicinity. The physically meaningful assumption of a unitary stoichiometry for a set of binding sites results in the increase by a factor of 2 in the dissociation constant (K_{D1}) of the high-affinity Zn^{2+} binding site in E295V compared

to that of the wild-type. Such an effect is consistent with a comparable increase in the value of the inhibitory constant (K_I), as evaluated from the Zn^{2+} inhibition kinetics (Figure 2). Together with the inhibition kinetics, the ITC analysis thus indicated that substitution of E295 to *V* weakens the binding of Zn^{2+} to the Q_o site of cyt bc_1, supporting the notion that E295 belongs to the metal ligand cluster.[24]

The dissociation constants and thermodynamic parameters provided in this study do not take into account possible events of proton transfer linked to metal binding, or the presence in solution of complexes between the metal ions and the buffer. This treatment is beyond the scope of this study. However, the values of the measured equilibrium constants compare well with those reported in the literature and determined using ITC or other methodologies, which, in principle, should also take into account similar effects. These values are therefore used only for comparison of native and mutant cyt bc_1 enzymes.

Redox-Induced FTIR Difference Spectroscopy. To investigate further whether Zn^{2+} inhibition occurs via E295 at the Q_o site of cyt bc_1, we performed the redox-induced FTIR difference spectra analyses using wild-type cyt bc_1, its E295V mutant, and a cyt bc_1 subcomplex lacking the Fe−S protein,[28] in the presence and absence of Zn^{2+} (Figure 4). The redox-induced FTIR difference spectra provide information about the protonation state of acidic residues or quinone binding, as described previously.[35,38,40,41] The positive and negative signals in the spectra correlate with the oxidized and reduced forms of the enzyme, respectively. Figure 4 shows an overview of the oxidized minus reduced FTIR difference spectra of wild-type cyt bc_1, the E295V mutant, and the cyt bc_1 subcomplex lacking the Fe−S protein. The spectra are dominated by signals from the free and bound quinones and include the amide I and amide II bands as well as signals from individual amino acids. Purified wild-type cyt bc_1 with and without Zn^{2+} retained their bound quinones as judged by their intense signals observed at 1288 and 1263 cm^{-1}, ascribed to the methoxy side chain (the C−O modes) of quinones. Alternatively, the signal at 1263 cm^{-1} may also be contributed indirectly by heme b_H or cyt c_1 $\delta(C_m-H)$ vibration. The spectral region between 1750 and 1700 cm^{-1} includes information about the protonated Asp/Glu residues and can be used as a good indicator of the environment of these redox active amino acids. The oxidation-induced protonation of acidic residues gives rise to a positive signal at 1739 cm^{-1}, which was previously assigned to the υ(C═O) vibration of D278 and E295 residues in cyt bc_1.[26,35,36,38,41] The negative signal observed at 1720 cm^{-1} can be assigned to the υ(C═O) vibration of protonated acidic residues. The presence of a pair of signals, 1739(+) cm^{-1} and 1720(−) cm^{-1}, is typical of the modification of the environment of redox active acidic residues upon redox reaction.[42] In fact, the higher the frequency, the more hydrophobic the environment of the acidic residue. The downshift of the negative signal indicates that the acidic residue is involved in stronger H-bonds or is more exposed to the solvent in the reduced form. This behavior points toward a conformational change of the residue upon redox reaction. A positive signal can be seen at 1706 cm^{-1}. This signal was tentatively assigned to an acidic residue located in the cyt *b* subunit of *Paracoccus denitrificans*.[38,43] Furthermore, this signal can arise also from the υ(C═O) vibration of the heme propionates. Upon addition of Zn^{2+}, the intensity of this signal decreased. In addition, the positive mode at 1739 cm^{-1} shifts to 1745 cm^{-1}, indicating that protonated Asp/Glu residues form stronger H-bonds upon

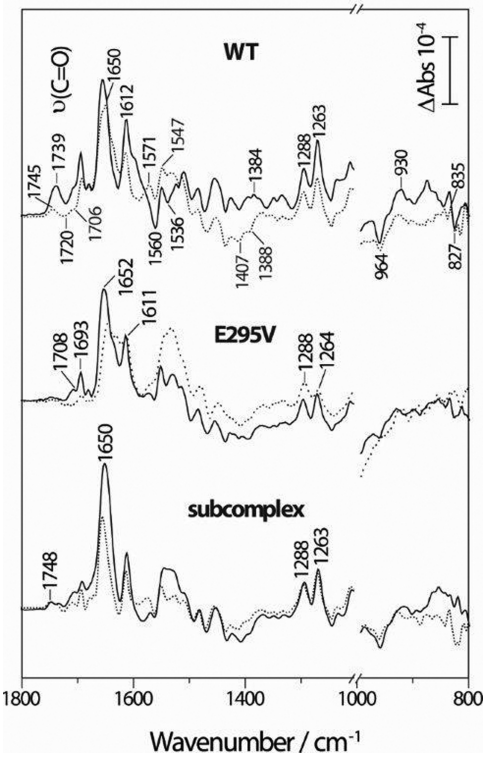

Figure 4. Oxidized minus reduced FTIR difference spectra of *R. capsulatus* wild-type cyt bc_1 (top), the E295V mutant (middle), and the cyt bc_1 subcomplex lacking the Fe−S protein subunit (bottom) in the absence (—) and presence (···) of 200 μM Zn^{2+} at pH 8.0. For further details, see the text.

reduction. Clearly, the FTIR spectra of wild-type cyt bc_1 showed direct interaction(s) between acidic residue(s) and Zn^{2+}.

Compared to the FTIR difference spectrum of the wild-type, the spectrum of the E295V mutant showed weaker signals in the spectral region for the protonated acidic residues, indicating that the E295 residue is responsible for the signals observed at 1739 and 1720 cm^{-1} in the difference spectrum of the wild-type. On the other hand, addition of Zn^{2+} to E295V did not show any redox-dependent signal as seen in the spectrum of the wild-type, suggesting that the E295 residue is a direct Zn^{2+} ligand as well as representing a proton exit group in cyt bc_1. The redox-dependent secondary structure modifications can be seen in the region of the amide I band.[44] The most prominent signal observed at 1650 cm^{-1}, assigned to the υ(C═O) vibrational mode of neutral fully oxidized quinones, was slightly altered by Zn^{2+} binding in the wild-type spectra, and in that for the E295V mutant enzyme, the signal was found to be slightly shifted and to have a larger half-width (Figure 4). The signals from the deprotonated heme propionates are expected in the so-called amide II region from 1560 to 1500 cm^{-1}, but they overlap with the side chain contribution of deprotonated acidic residues.[41,43] Note that these contributions could be seen as negative signals in the difference spectra at 1560 and 1536 cm^{-1} for wild-type cyt bc_1. The positive signal at 1547 cm^{-1} can be assigned to the amide II vibration as well as to the υ_{38} vibration of heme b_L. Upon Zn^{2+} inhibition, a positive signal appears in the difference spectrum at 1571 cm^{-1} that can be assigned to the $\upsilon(COO^-)^{as}$ vibration of deprotonated acidic residues. This signal could arise from the acidic residues that bind Zn^{2+}. This observation leads to the conclusion

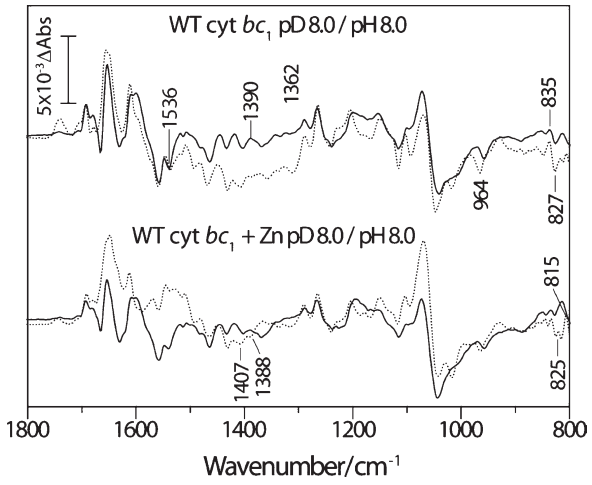

Figure 5. Effects of H−D exchange on the FTIR difference spectra of wild-type cyt bc_1 in the absence and presence of 200 μM Zn^{2+}: (top) FTIR difference spectra of wild-type cyt bc_1 recorded at pD 8.0 (—) and pH 8.0 (···) and (bottom) FTIR difference spectra of wild-type cyt bc_1 in the presence of Zn^{2+} recorded at pD 8.0 (—) and pH 8.0 (···). See the text for further details.

that the relevant acidic residue binds Zn^{2+} via its carboxyl moiety.

H−D exchange leads to an uncoupling and downshift of the amide II band to ~1450 cm^{-1}, thus clarifying the signature of the deprotonated acidic residues as well as the heme propionates. The difference spectra of the wild-type and Zn^{2+}-inhibited cyt bc_1 recorded at pD 8.0 are presented in Figure 5. These spectra show that the signal observed at 1536 cm^{-1} in the difference spectrum of the wild-type is absent after H−D exchange. Indeed, this signal arises from the amide II modes, downshifted upon H−D exchange. Another major spectral change was observed at ≤1400 cm^{-1}, at 1390, 1384, and 1362 cm^{-1} in the wild-type. These signals include the coordinates from the quinone ring motions, $\upsilon(COO^-)^s$ of Asp/Glu (heme b_H) or the heme propionate. When Zn^{2+} bound to cyt bc_1, only two signals at 1407 and 1388 cm^{-1} remained visible in the spectrum. However, in the spectrum of the E295V mutant enzyme, no signal was evident in this spectral region, indicating that there was no effect of Zn^{2+} binding on the E295 residue and the hemes.

The specific porphyrin ring motions can be observed between 1000 and 800 cm^{-1} and are sensitive to pH.[34,45,46] The difference spectrum of the wild-type contains a negative signal at 964 cm^{-1} and a positive signal at 930 cm^{-1}, assigned to the ring deformation vibration of the imidazole.[47,48] It is thus likely that the coordinating His of the heme groups gives rise to these signals. Upon addition of Zn^{2+}, these signals lose intensity, suggesting that the relevant His residue(s) is not perturbed by the reaction any longer. The redox sensitive signal appearing at 835 cm^{-1} is shifted toward 827 cm^{-1} upon reduction. This signal was previously assigned to the $\gamma(C_m-H)$ vibration of the porphyrin ring.[34] The frequency of the $\gamma(C_m-H)$ vibration depends also on the pH. At high pH, the 835 cm^{-1} signal is found at a high frequency, and at low pH, it is found at a low frequency (i.e., 827 cm^{-1}). This behavior indicates that the heme propionates are in the protonated state in the oxidized form and deprotonated in the reduced state. The inhibition induces the splitting of the negative signal into two signals at 825 and 815 cm^{-1}. Thus, the

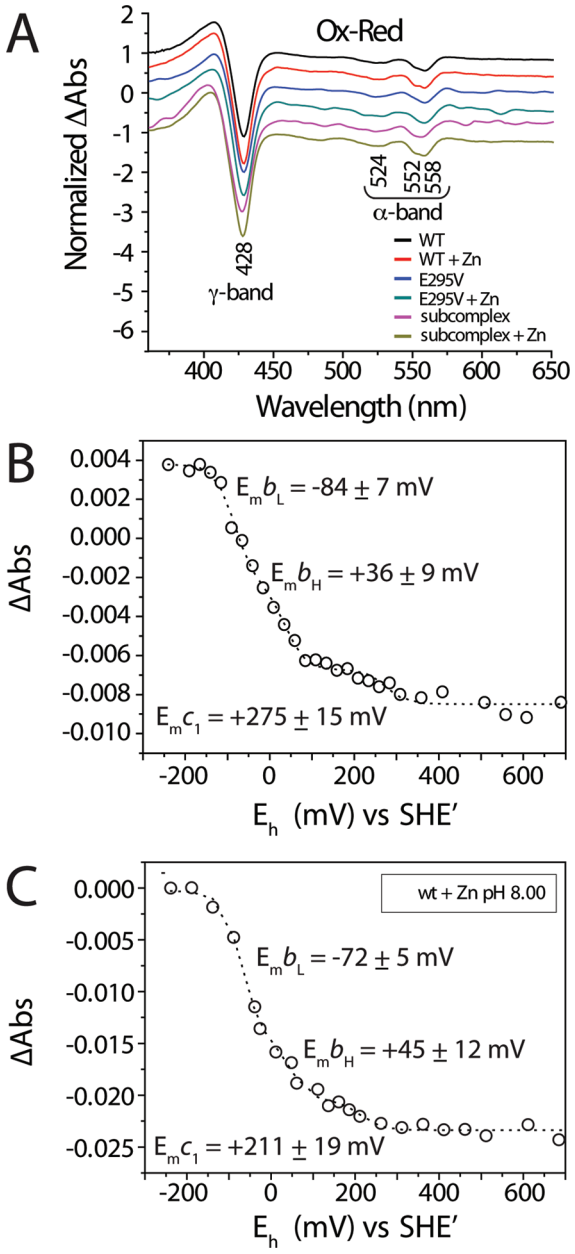

Figure 6. Redox midpoint potentials of heme cofactors of wild-type cyt bc_1 in the absence and presence of Zn^{2+}. UV−vis optical absorbance difference spectra (A) of the wild-type, E295V, and the cyt bc_1 subcomplex lacking the Fe−S protein in the presence and absence of 200 μM Zn^{2+}. Voltametric redox equilibrium titrations of heme cofactors of wild-type cyt bc_1 in the absence (B) and presence (C) of 200 μM Zn^{2+}. Potentiometric titrations were performed in 100 mM Tris-HCl and 100 mM KCl (pH 8.0). The E_{m7} values for cyt c_1 and cyt b obtained from the absorption difference in the Soret region (γ-band at 428 nm in panel A) and the normalized data were fit to a Nernst equation with three n = 1 components. Mediators were used as described for the FTIR studies.

addition of Zn^{2+} modifies the protonation state of the propionates and/or the His that coordinate the iron of the hemes. The heme signature of the E295V mutant is similar to that observed for the inhibited wild-type, indicating that this mutation has an effect similar to the effect of inhibition on the protonation state of the hemes.

dx.doi.org/10.1021/bi200230e |*Biochemistry* 2011, 50, 4263–4272

UV−Vis Difference Spectroscopy and Titration of cyt bc_1 Hemes. The UV−vis redox difference spectra of the wild-type, the E295V mutant, and the cyt bc_1 subcomplex lacking the Fe−S protein were compared in the presence and absence of Zn^{2+} with respect to the γ-band at 428 nm and α-bands at 524, 552, and 558 nm (Figure 6A). All enzymes were fully oxidized in 5 min at 500 mV versus SHE and fully reduced within 7 min at −500 mV versus SHE, indicating that either mutating E295 or the absence of the Fe−S protein does not affect the redox behavior of hemes *b* and c_1 of cyt bc_1 (Figure 6A). On the other hand, addition of Zn^{2+} slowed the reduction observed as the fully reduced samples were obtained 10 min after the application of the reducing potential (data not shown) while the oxidation rate remained unaffected.

UV−vis titrations were performed by monitoring the absorbance of the Soret band of the wild-type enzyme in the presence and absence of Zn^{2+} to determine the effect of Zn^{2+} binding on the midpoint potentials of the hemes of cyt bc_1 (Figure 6B,C). The oxidative titration curves showed that Zn^{2+} inhibition does not significantly affect the midpoint potentials of the *b*-type hemes, whereas the midpoint potential of E295V mutant heme c_1 seemed to be slightly shifted in the presence of Zn^{2+}. However, we note that the equilibration time is typically very long for heme c_1, leading to an error larger than that seen for the other hemes.

DISCUSSION

The vectorial translocation of protons across the membrane for the generation of ΔpH involves cyt bc_1, whose proton transfer pathways are not well defined. The E295 residue found in the highly conserved PEWY motif of the cyt *b* subunit of cyt bc_1 might play an important role in the release of protons when QH_2 oxidation occurs. Clearly, mutation of this residue affects the electron transferring activity of cyt bc_1 as shown in several studies with bovine, yeast, and bacterial cyt bc_1.[17,26,36,37] Nevertheless, its role in either Q−QH_2 binding for the formation of the enzyme−substrate (ES) complex[17,36] or proton release associated with H_2O molecules near the Q_o site[26,37,38] remained less clear. Considering these possibilities, here we performed Zn^{2+} inhibition studies using steady-state kinetics, ITC analysis, and redox-induced difference FTIR spectroscopy with both the native form and the E295V mutant derivative of cyt bc_1.

The kinetic parameters of cyt bc_1 were obtained as a first approximation using a simple Michaelis−Menten kinetics with DBH_2 as a substrate to compare the E295V mutant with the wild-type enzyme under steady-state conditions (Table 1). E295V has a 4-fold lower V_{max} value than the wild-type, whereas its K_m value for DBH_2 was only marginally lower. Thus, its lower V_{max} affected its apparent catalytic efficiency, V_{max}/K_m. Previously, E295 was proposed to be an important residue for the formation of an ES complex at the Q_o site through formation of a H-bond with the OH group of stigmatellin that might mimic a reaction intermediate (i.e., either SQ or QH_2) based on the crystal structures of cyt bc_1.[17,36] However, substitution of E295 with various amino acids revealed a robustness of the cyt bc_1 electron transferring activity,[26] suggesting that this residue may not be involved in substrate binding to form the ES complex but might rather influence later steps of proton transfer directly or indirectly.[37] This suggestion was confirmed by our kinetic data (Table 1). Indeed, addition of Zn^{2+} in the micromolar concentration range severely inhibited wild-type cyt bc_1, whereas E295V, featuring a K_I value 4-fold higher than that of the wild-type, was less sensitive to Zn^{2+} (Figure 2). These kinetic results, pointing to a role of E295 in the inhibitory binding of Zn^{2+}, are consistent with cyt bc_1 metal binding properties determined by ITC (Figure 3). Indeed, in wild-type cyt bc_1, ITC analysis showed the presence of a high-affinity Zn^{2+} binding site, characterized by a dissociation constant (K_D) on the same order of magnitude as the inhibitory constant (K_I) derived from the kinetic study under similar conditions. Interestingly, a similar matching between the K_D of the high-affinity Zn^{2+} binding site and K_I has been previously observed for bovine cyt bc_1, using a different approach to determine the binding parameters, under the conditions tested.[39] As observed in eukaryotic cyt bc_1,[39] in the case of bacterial cyt bc_1, the ITC analysis revealed additional Zn^{2+} binding sites that are characterized by a dissociation constant 10 times higher than that of the inhibitory high-affinity site. These sites are likely to reflect less specific interactions with the metal ion and are unrelated to Zn^{2+} inhibition of the catalytic activity. Furthermore, analysis of the data of the titration effected with the E295V mutant indicates that the Zn^{2+} binding is weakened compared to that of the wild-type, paralleling the weaker inhibition observed in the kinetic studies. Consequently, both kinetic and ITC data support the previous proposal based on EXAFS analysis[24] that E295 is one of the Zn^{2+} ligands, further suggesting that the E295 residue, as the Zn^{2+} ligand, is involved in the release of protons by cyt bc_1.

We further investigated the involvement of residue E295 in Zn^{2+} binding using both redox-induced FTIR difference and UV−visible redox difference spectra of the wild-type and E295V mutant complex in the absence and presence of Zn^{2+}, and we determined the midpoint potentials of heme *b* and *c* cofactors of cyt bc_1 (Figure 6). The electron transfer rate reflected by the redox behavior of cyt *b* and cyt *c* showed that Zn^{2+} slowed the electron transfer activity of cyt bc_1. This was also supported by the observation that the typical infrared signature (<1000 cm^{-1}) of the porphyrin ring of the Zn^{2+}-bound wild-type enzyme was similar to that of E295V without Zn^{2+}, indicating that E295 might provide favorable conformational changes for the occurrence of bifurcated electron transfer at the Q_o site. However, the loss of such changes, due to the presence of Zn^{2+} or the E to V substitution, did not alter the redox potentials of heme *b* and c_1 cofactors even in the presence of Zn^{2+} (Figure 6B,C). Thus, these data indicated that neither substrate binding (K_m) nor ES complex formation (lower E_a) requires E295 necessarily.[17] Rather, as previously suggested,[26,37] upon binding and oxidation of QH_2 at the Q_o site, this residue seems to contribute to the formation of a pathway associated with H_2O for proton release during Q_o catalysis. Regardless of the presence or absence of Zn^{2+}, substitution of E295 weakened the signals of the protonated acidic residue in both oxidized and reduced forms (at 1746 and 1722 cm^{-1}, respectively) as well as the signals of deprotonated residues in the reduced form, typically observed in the wild-type. On the other hand, the wild-type enzyme inhibited by Zn^{2+} also lost these signals, indicating that Zn^{2+} interfered directly with protonation and deprotonation of E295 in cyt bc_1. In addition, Zn^{2+} could bind the E295 residue directly via the carboxylate moiety as observed from the $\upsilon(COO^-)$ vibrational mode at 1560 cm^{-1} (Figure 4). Earlier FTIR studies showed that in *P. denitrificans* cyt bc_1 bound to stigmatellin, E295 is H-bonded to the carbonyl group of this inhibitor in the oxidized form.[38] The FTIR spectroscopic data strongly suggested that protonation and deprotonation of E295 might be important for displacement of its carboxylate side chain at the Q_o site, resulting in the modification of the relative hydrophobicity of the Q_o cavity

facing the outer membrane surface, which is strongly associated with H_2O molecules. Consequently, it appears that a perturbed protonation and deprotonation state of E295, by either mutation or Zn^{2+} binding, prevents a facilitated movement of the side chain of this residue toward the propionate group of heme b_L. This would hamper the rapid release of a proton from the Q_o site, resulting in slower electron transfer to the low-potential chain.

Notably, the removal of the Fe−S protein from the cyt bc_1 induced inaccessibility of Zn^{2+} to E295 (Figure 4). Although the Fe−S protein is not likely to participate in Zn^{2+} binding directly, it is possible that a conformational change in the *ef* loop, due to the absence of the Fe−S protein, might drastically modify the location of the PEWY motif, resulting in the displacement of E295 toward the more hydrophobic inner portion of the membrane, hampering Zn^{2+} accessibility. Other cyt *b* residues such as H276, D278, and N279 that act as ligands to Zn^{2+} were additionally proposed to act as proton exit paths on the basis of EXAFS studies.[24] Recent FTIR data with D278 in *P. denitrificans* cyt bc_1 indicated that even in the presence of stigmatellin, this residue remains protonated in the oxidized form, but its vibrational frequency shifts in the reduced form.[38] Therefore, the role of these residues in proton pathways of cyt bc_1 needs to be examined using site-directed mutagenesis coupled to an analogous experimental approach as described here. These studies are underway in our laboratories.

AUTHOR INFORMATION

Corresponding Author

*Telephone: (215) 898-4394. Fax: (215) 898-8780. E-mail: fdaldal@sas.upenn.edu.

Present Addresses

⊥Industrial Biotechnology and Bioenergy Research Center, Korea Research Institute of Bioscience and Biotechnology, Daejeon, Korea 305-806.

Funding Sources

This work was supported by grants to F.D. from the National Institutes of Health (GM 38237) and the Department of Energy (91ER 20052). G.V. and F.F. acknowledge financial support by MIUR of Italy (Grants PRIN 2008ZWHZJT and PRIN 2008XB774B), and P.H. and Y.E.K. acknowledge financial support from the ANR Chaire d'Excellence and CNRS.

ACKNOWLEDGMENT

The VP-ITC instrument is the property of CIRB-UniBO.

ABBREVIATIONS

cyt, cytochrome; cyt bc_1, ubihydroquinone:cyt *c* oxidoreductase; Fe−S, iron−sulfur; Q_o, hydroquinone oxidation; Q_i, quinone reduction; QH_2, hydroquinone; Q, quinone; SQ, semiquinone; MPYE, mineral-peptone-yeast extract; MOPS, 4-morpholinepropanesulfonic acid; DBH_2, decylbenzohydroquinone; DDM, dodecyl maltoside; EPR, electron paramagnetic resonance; ITC, isothermal titration calorimetry; FTIR, Fourier transform infrared; EXAFS, extended X-ray absorption fine structure; DCCD, dicyclohexylcarbodiimide.

REFERENCES

(1) Papa, S., Lorusso, M., and Di Paola, M. (2006) Cooperativity and flexibility of the protonmotive activity of mitochondrial respiratory chain. *Biochim. Biophys. Acta 1757*, 428–436.

(2) Trumpower, B. L. (1990) The protonmotive Q cycle. Energy transduction by coupling of proton translocation to electron transfer by the cytochrome bc_1 complex. *J. Biol. Chem. 265*, 11409–11412.

(3) Berry, E. A., Guergova-Kuras, M., Huang, L. S., and Crofts, A. R. (2000) Structure and function of cytochrome *bc* complexes. *Annu. Rev. Biochem. 69*, 1005–1075.

(4) Darrouzet, E., Cooley, J. W., and Daldal, F. (2004) The cytochrome bc_1 complex and its homologue the b_6f complex: Similarities and differences. *Photosynth. Res. 79*, 25–44.

(5) Iwata, S., Lee, J. W., Okada, K., Lee, J. K., Iwata, M., Rasmussen, B., Link, T. A., Ramaswamy, S., and Jap, B. K. (1998) Complete structure of the 11-subunit bovine mitochondrial cytochrome bc_1 complex. *Science 281*, 64–71.

(6) Darrouzet, E., Moser, C. C., Dutton, P. L., and Daldal, F. (2001) Large scale domain movement in cytochrome bc_1: A new device for electron transfer in proteins. *Trends Biochem. Sci. 26*, 445–451.

(7) Zhang, Z., Huang, L., Shulmeister, V. M., Chi, Y. I., Kim, K. K., Hung, L. W., Crofts, A. R., Berry, E. A., and Kim, S. H. (1998) Electron transfer by domain movement in cytochrome bc_1. *Nature 392*, 677–684.

(8) Xia, D., Yu, C. A., Kim, H., Xia, J. Z., Kachurin, A. M., Zhang, L., Yu, L., and Deisenhofer, J. (1997) Crystal structure of the cytochrome bc_1 complex from bovine heart mitochondria. *Science 277*, 60–66.

(9) Jenney, F. E., Jr., Prince, R. C., and Daldal, F. (1996) The membrane-bound cytochrome c_y of *Rhodobacter capsulatus* can serve as an electron donor to the photosynthetic reaction of *Rhodobacter sphaeroides*. *Biochim. Biophys. Acta 1273*, 159–164.

(10) Jenney, F. E., Jr., Prince, R. C., and Daldal, F. (1994) Roles of the soluble cytochrome c_2 and membrane-associated cytochrome c_y of *Rhodobacter capsulatus* in photosynthetic electron transfer. *Biochemistry 33*, 2496–2502.

(11) Jenney, F. E., Jr., and Daldal, F. (1993) A novel membrane-associated *c*-type cytochrome, cyt c_y, can mediate the photosynthetic growth of *Rhodobacter capsulatus* and *Rhodobacter sphaeroides*. *EMBO J. 12*, 1283–1292.

(12) Gray, K. A., Dutton, P. L., and Daldal, F. (1994) Requirement of histidine 217 for ubiquinone reductase activity (Q_i site) in the cytochrome bc_1 complex. *Biochemistry 33*, 723–733.

(13) Wang, Y., Obungu, V., and Beattie, D. S. (1998) Dicyclohexylcarbodiimide inhibits proton pumping in ubiquinol:cytochrome *c* oxidoreductase of *Rhodobacter sphaeroides* and binds to aspartate-187 of cytochrome *b*. *Arch. Biochem. Biophys. 352*, 193–198.

(14) Shinkarev, V. P., Ugulava, N. B., Crofts, A. R., and Wraight, C. A. (2000) DCCD inhibits the reactions of the iron-sulfur protein in *Rhodobacter sphaeroides* chromatophores. *Biochemistry 39*, 16206–16212.

(15) Shinkarev, V. P., Ugulava, N. B., Takahashi, E., Crofts, A. R., and Wraight, C. A. (2000) Aspartate-187 of cytochrome *b* is not needed for DCCD inhibition of ubiquinol:cytochrome *c* oxidoreductase in *Rhodobacter sphaeroides* chromatophores. *Biochemistry 39*, 14232–14237.

(16) Wang, Y., and Beattie, D. S. (2002) Molecular modeling studies of the DCCD-treated cytochrome bc_1 complex: Predicted conformational changes and inhibition of proton translocation. *J. Bioenerg. Biomembr. 34*, 81–88.

(17) Crofts, A. R., Hong, S., Ugulava, N., Barquera, B., Gennis, R., Guergova-Kuras, M., and Berry, E. A. (1999) Pathways for proton release during ubihydroquinone oxidation by the bc_1 complex. *Proc. Natl. Acad. Sci. U.S.A. 96*, 10021–10026.

(18) Utschig, L. M., Ohigashi, Y., Thurnauer, M. C., and Tiede, D. M. (1998) A new metal-binding site in photosynthetic bacterial reaction centers that modulates Q_A to Q_B electron transfer. *Biochemistry 37*, 8278–8281.

(19) Giachini, L., Francia, F., Mallardi, A., Palazzo, G., Carpene, E., Boscherini, F., and Venturoli, G. (2005) Multiple scattering X-ray absorption studies of Zn^{2+} binding sites in bacterial photosynthetic reaction centers. *Biophys. J. 88*, 2038–2046.

(20) Adelroth, P., Paddock, M. L., Sagle, L. B., Feher, G., and Okamura, M. Y. (2000) Identification of the proton pathway in bacterial reaction centers: Both protons associated with reduction of Q_B to Q_BH_2 share a common entry point. *Proc. Natl. Acad. Sci. U.S.A. 97*, 13086–13091.

(21) Axelrod, H. L., Abresch, E. C., Paddock, M. L., Okamura, M. Y., and Feher, G. (2000) Determination of the binding sites of the proton transfer inhibitors Cd^{2+} and Zn^{2+} in bacterial reaction centers. *Proc. Natl. Acad. Sci. U.S.A. 97*, 1542–1547.

(22) Qin, L., Mills, D. A., Hiser, C., Murphree, A., Garavito, R. M., Ferguson-Miller, S., and Hosler, J. (2007) Crystallographic location and mutational analysis of Zn and Cd inhibitory sites and role of lipidic carboxylates in rescuing proton path mutants in cytochrome *c* oxidase. *Biochemistry 46*, 6239–6248.

(23) Mills, D. A., Schmidt, B., Hiser, C., Westley, E., and Ferguson-Miller, S. (2002) Membrane potential-controlled inhibition of cytochrome *c* oxidase by zinc. *J. Biol. Chem. 277*, 14894–14901.

(24) Giachini, L., Francia, F., Veronesi, G., Lee, D. W., Daldal, F., Huang, L. S., Berry, E. A., Cocco, T., Papa, S., Boscherini, F., and Venturoli, G. (2007) X-ray absorption studies of Zn^{2+} binding sites in bacterial, avian, and bovine cytochrome bc_1 complexes. *Biophys. J. 93*, 2934–2951.

(25) Berry, E. A., Zhang, Z., Bellamy, H. D., and Huang, L. (2000) Crystallographic location of two Zn^{2+}-binding sites in the avian cytochrome bc_1 complex. *Biochim. Biophys. Acta 1459*, 440–448.

(26) Osyczka, A., Zhang, H., Mathe, C., Rich, P. R., Moser, C. C., and Dutton, P. L. (2006) Role of the PEWY glutamate in hydroquinone-quinone oxidation-reduction catalysis in the Q_o site of cytochrome bc_1. *Biochemistry 45*, 10492–10503.

(27) Atta-Asafo-Adjei, E., and Daldal, F. (1991) Size of the amino acid side chain at position 158 of cytochrome *b* is critical for an active cytochrome bc_1 complex and for photosynthetic growth of *Rhodobacter capsulatus*. *Proc. Natl. Acad. Sci. U.S.A. 88*, 492–496.

(28) Valkova-Valchanova, M. B., Saribas, A. S., Gibney, B. R., Dutton, P. L., and Daldal, F. (1998) Isolation and characterization of a two-subunit cytochrome b-c_1 subcomplex from *Rhodobacter capsulatus* and reconstitution of its ubihydroquinone oxidation (Q_o) site with purified Fe-S protein subunit. *Biochemistry 37*, 16242–16251.

(29) Lee, D. W., Ozturk, Y., Osyczka, A., Cooley, J. W., and Daldal, F. (2008) Cytochrome bc_1-c_y fusion complexes reveal the distance constraints for functional electron transfer between photosynthesis components. *J. Biol. Chem. 283*, 13973–13982.

(30) Smith, P. K., Krohn, R. I., Hermanson, G. T., Mallia, A. K., Gartner, F. H., Provenzano, M. D., Fujimoto, E. K., Goeke, N. M., Olson, B. J., and Klenk, D. C. (1985) Measurement of protein using bicinchoninic acid. *Anal. Biochem. 150*, 76–85.

(31) Laemmli, U. K. (1970) Cleavage of structural proteins during the assembly of the head of bacteriophage T4. *Nature 227*, 680–685.

(32) Rich, P. R. (1984) Electron and proton transfers through quinones and cytochrome *bc* complexes. *Biochim. Biophys. Acta 768*, 53–79.

(33) Moss, D., Nabedryk, E., Breton, J., and Mantele, W. (1990) Redox-linked conformational changes in proteins detected by a combination of infrared spectroscopy and protein electrochemistry. Evaluation of the technique with cytochrome *c*. *Eur. J. Biochem. 187*, 565–572.

(34) Dorr, S., Wolpert, M., and Hellwig, P. (2006) Study on the redox state dependent γ(CH) vibrational modes of the *c*-type heme. *Biopolymers 82*, 349–352.

(35) Ritter, M., Palsdottir, H., Abe, M., Mantele, W., Hunte, C., Miyoshi, H., and Hellwig, P. (2004) Direct evidence for the interaction of stigmatellin with a protonated acidic group in the bc_1 complex from *Saccharomyces cerevisiae* as monitored by FTIR difference spectroscopy and ^{13}C specific labeling. *Biochemistry 43*, 8439–8446.

(36) Wenz, T., Hellwig, P., MacMillan, F., Meunier, B., and Hunte, C. (2006) Probing the role of E272 in quinol oxidation of mitochondrial complex III. *Biochemistry 45*, 9042–9052.

(37) Seddiki, N., Meunier, B., Lemesle-Meunier, D., and Brasseur, G. (2008) Is cytochrome *b* glutamic acid 272 a quinol binding residue in the bc_1 complex of *Saccharomyces cerevisiae*? *Biochemistry 47*, 2357–2368.

(38) Kleinschroth, T., Anderka, O., Ritter, M., Stocker, A., Link, T. A., Ludwig, B., and Hellwig, P. (2008) Characterization of mutations in crucial residues around the Q_o binding site of the cytochrome *bc* complex from *Paracoccus denitrificans*. *FEBS J. 275*, 4773–4785.

(39) Link, T. A., and von Jagow, G. (1995) Zinc ions inhibit the Q_P center of bovine heart mitochondrial bc_1 complex by blocking a protonatable group. *J. Biol. Chem. 270*, 25001–25006.

(40) Iwaki, M., Giotta, L., Akinsiku, A. O., Schagger, H., Fisher, N., Breton, J., and Rich, P. R. (2003) Redox-induced transitions in bovine cytochrome bc_1 complex studied by perfusion-induced ATR-FTIR spectroscopy. *Biochemistry 42*, 11109–11119.

(41) Baymann, F., Robertson, D. E., Dutton, P. L., and Mantele, W. (1999) Electrochemical and spectroscopic investigations of the cytochrome bc_1 complex from *Rhodobacter capsulatus*. *Biochemistry 38*, 13188–13199.

(42) Hellwig, P., Behr, J., Ostermeier, C., Richter, O. M., Pfitzner, U., Odenwald, A., Ludwig, B., Michel, H., and Mantele, W. (1998) Involvement of glutamic acid 278 in the redox reaction of the cytochrome *c* oxidase from *Paracoccus denitrificans* investigated by FTIR spectroscopy. *Biochemistry 37*, 7390–7399.

(43) Ritter, M., Anderka, O., Ludwig, B., Mantele, W., and Hellwig, P. (2003) Electrochemical and FTIR spectroscopic characterization of the cytochrome bc_1 complex from *Paracoccus denitrificans*: Evidence for protonation reactions coupled to quinone binding. *Biochemistry 42*, 12391–12399.

(44) Kong, J., and Yu, S. (2007) Fourier transform infrared spectroscopic analysis of protein secondary structures. *Acta Biochim. Biophys. Sin. 39*, 549–559.

(45) Dorr, S., Schade, U., and Hellwig, P. (2008) Far infrared spectroscopy on hemoproteins: A model compound study from 1800−100 cm^{-1}. *Vib. Spectrosc. 47*, 59–65.

(46) Berthomieu, C., Marboutin, L., Dupeyrat, F., and Bouyer, P. (2006) Electrochemically induced FTIR difference spectroscopy in the mid- to far infrared (200 μm) domain: A new setup for the analysis of metal-ligand interactions in redox proteins. *Biopolymers 82*, 363–367.

(47) Hasegawa, K., Ono, T., and Noguchi, T. (2000) Vibrational spectra and ab initio DFT calculations of 4-methylimidazole and its different protonation forms: Infrared and Raman markers of the protonation state of a histidine side chain. *J. Phys. Chem. B 104*, 4253–4265.

(48) Wolpert, M., and Hellwig, P. (2006) Infrared spectra and molar absorption coefficients of the 20 α amino acids in aqueous solutions in the spectral range from 1800 to 500 cm^{-1}. *Spectrochim. Acta, Part A 64*, 987–1001.

(49) Berry, E. A., Huang, L. S., Saechao, L. K., Pon, N. G., Valkova-Valchanova, M., and Daldal, F. (2004) X-ray structure of *Rhodobacter capsulatus* cytochrome bc_1: Comparison with its mitochondrial and chloroplast counterparts. *Photosynth. Res. 81*, 251–275.

(50) Gazaryan, I. G., Krasnikov, B. F., Ashby, G. A., Thorneley, R. N., Kristal, B. S., and Brown, A. M. (2002) Zinc is a potent inhibitor of thiol oxidoreductase activity and stimulates reactive oxygen species production by lipoamide dehydrogenase. *J. Biol. Chem. 277*, 10064–10072.